NUMERICAL ANALYSIS OF BULK DRAG COEFFICIENT IN DENSE VEGETATION BY IMMERSED BOUNDARY METHOD

Tomohiro Suzuki[1] and Taro Arikawa[2]

In this paper, bulk drag coefficient in rigid dense vegetation is investigated mainly by using a three dimensional numerical simulation model CADMAS-SURF/3D by incorporating Immersed Boundary Method to calculate flow around the vertical cylinder in the Cartesian grid. Large Eddy Simulation is also incorporated as a turbulence model. Firstly, validation of the developed model is conducted with a single cylinder in the flow field based on literature. All the results obtained here (Re=300, 3,900 and 8,000) show good agreement with the reference data in literature. After the validation, multiple cylinders are allotted in three different densities (S/D=2.8, 2.0, 1.4) in a numerical wave tank and numerical simulations are conducted to investigate bulk drag coefficient. The result shows that the ratio of bulk drag coefficient to drag coefficient, which represents a reduction, is not just a function of density but a function of parameter $2a/S$, in which $2a$ is stroke of the motion and S is cylinder distance. $2a$ is less than S, the effect of the density is neglected because the wake does not reach the other cylinders even when the density is high. On the contrary, it might affect the ratio of bulk drag coefficient to drag coefficient when the stroke of the motion is larger than the cylinder distance even when the density is low. In general, the ratio of bulk drag coefficient to drag coefficient decreases when $2a/S$ increases.

Keywords: bulk drag coefficient; drag coefficient; multiple cylinders; vegetation; Immersed Boundary Method; CADMAS-SURF/3D; Large Eddy Simulation

INTRODUCTION

The function of coastal vegetation as shoreline defenses is attracting engineers' attentions with an increasing interest in sea level rise and the increasing importance of eco- or soft-engineering for coastal engineering in recent times. Coastal vegetation such as mangrove forests and salt marshes affords coastal protection by reducing wave energy. An important process is wave energy dissipation due to the cylindrical structures that vegetation forms. The vegetation imposes drag and friction forces on the water motion, which results in energy loss in waves. Understanding the hydraulic processes in vegetation fields is important for the protection of highly populated areas behind it, for the preservation of the vegetation as well as for the estimation of erosion potential in and around the vegetation.

However, the wave dissipation effect in vegetated fields has not been fully clarified yet. To understand the wave dissipation, it would be important to understand bulk drag coefficient appropriately, which is strongly related to turbulence structure in multiple cylinders in the waves. It is not a trivial task to obtain bulk drag coefficients in different hydraulic and vegetation conditions without calibration but it is assumed to be possible for a case of a simple array of rigid cylinders. Looking into practice, many authors (e.g. Iimura et al. 2007, Narayan 2009, de Oude et al. 2010) supposed bulk drag coefficient of vertical rigid cylinders to be 1.0 in the case of a simple cylindrical array (e.g. Mangrove forest) in subcritical flow regime Reynolds number. This value, C_D=1.0, is decided based on flow conditions and is being applied for wave conditions. This choice though practical, lacks background theories which support this value. For instance, drag coefficient of single cylinder in planar oscillations varies from 0.5 to 2.5 according to Sarpkaya (1976) and is quite sensitive to hydraulic parameters such as Reynolds number, Keulegan-Carpenter number and beta (frequency parameter). Not only that, the value can be different in the case of multiple cylinders. For example, according to experimental studies by Heideman and Sarpkaya (1985), drag coefficient in an array of cylinders is smaller than the drag coefficient for a single cylinder in an oscillatory flow. Nepf (1999) also shows that the bulk drag coefficient in a flow changes drastically with different cylinder density. Massel et al. (1999) propose an estimation method to calculate bulk drag coefficient depending on mangrove density by using a modification parameter based on the drag coefficient in SPM (1984). Considering these results, it is assumed that bulk drag coefficient in an array of cylinders under wave condition is smaller than for a single cylinder. Mangrove forests and salt marshes are often densely vegetated, so it would be important to understand bulk drag coefficient in dense vegetation conditions under wave conditions, which may not be the same as drag coefficient in a single cylinder.

[1] Faculty of Civil Engineering and Geosciences, Delft University of Technology, Stevinweg 1, 2628 CN DELFT, The Netherlands.
[2] Maritime structure division, Port and Airport Research Institute, 3-1-1 Nagase, Yokosuka 239-0826, Japan.

In this paper, the relationship between bulk drag coefficient and cylinder density based on hydrodynamics in multiple cylinders is investigated.

To this end, a three-dimensional numerical simulation based on Navier-Stokes equation is supposed as being useful, since a physical experiment often has some limitations for measurements in such dense vegetation. As a numerical model, the three-dimensional VOF model CADMAS-SURF/3D (Arikawa et al., 2005, Arikawa et al., 2007) developed by P.A.R.I. - whose usefulness in vegetation studies was suggested by Suzuki et al. (2009) - is used in this study. However, the wake of a circular cylinder was not fully represented by the porous model approach and the coarse grids in Suzuki et al. (2009). In order to improve the calculation of the hydrodynamics around the circular cylinder, Immersed Boundary Method (e.g. Baralas 2004, Peskin 1972) which can deal with arbitrary boundaries in a Cartesian grid, and Large Eddy Simulation (e.g. Christensen and Deigaard 2001, Suzuki and Okayasu 2004) as a turbulence model are incorporated in this study. By using these methods, the relationship between bulk drag coefficients and density, which supposes to be crucial to the estimation of the wave dissipation by vegetation, is studied.

MODEL

Immersed Boundary Method

Immersed Boundary Method has been developed to calculate flow around an arbitrary shape in a Cartesian grid. This method was originally introduced by Peskin (1972) and is used to investigate the interaction of flow and structure. Since then, some different methods have been proposed to calculate the force around a structure. One of them is to use feedback forcing (Peskin 1972, Briscolini 1989, Goldstein et al. 1993), and the other one is to use direct forcing (Mohd-Yusof 1997, Fadlun et al. 2000, Balaras 2004, Yang and Balaras 2006). In this study, the direct forcing method as used in Balaras (2004) is applied.

Advantages in applying Immersed Boundary Method in this study are 1) easy to incorporate into existing models such as the CADMAS-SURF/3D, 2) applicable to multiple cylinders whereas body fitted curvilinear grid is not suitable to them, 3) can be extended to the study of flexible plants and 4) easy to create the calculation grid because of the Cartesian grid as opposed to an unstructured grid which takes a lot of time to produce.

The calculation method for a fixed circular cylinder in this study is as follows. First, each velocity calculation point in the Cartesian grid is divided into three categories, namely, one inside the cylinder, one outside the cylinder and one outside the cylinder but on a tangent to the cylinder surface. The velocity point in the last category is called Ghost cell (point G), which is the interpolation point shown in Figure 1 and Figure 2. Next, a normal line from point G to the cylinder surface is drawn and the cross point is set as point A in which the velocity value is zero. Subsequently, the position of point I is decided by the method described in Balaras (2004) and the value of point I is calculated by a standard bilinear interpolation using the values of point B, C, D. Finally the velocity at point G is decided based on the wall modeling as shown in Figure 3 and described in the following equations. After that, the interpolated velocity is used to calculate the external body force on the immersed boundary. Thus an external body force is designed to enforce the proper boundary conditions on a circular cylinder in the Cartesian grid in this study. Note that the interpolation scheme here is two-dimensional because the shape of the circular cylinder which is used in this study is uniform along the vertical axis.

$$u_+ = z_+ \qquad (z_+ \le 5 : \text{viscous sub-layer}) \qquad (1)$$

$$u_+ = 5.0 \log z_+ - 3.05 \qquad (5 < z_+ \le 30 : \text{buffer layer}) \qquad (2)$$

$$u_+ = 2.5 \log z_+ - 5.5 \qquad (30 < z_+ : \text{Log-law region}) \qquad (3)$$

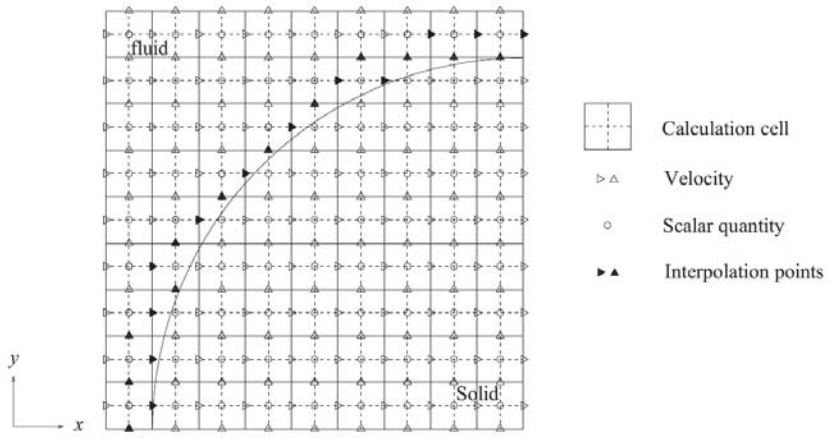

Figure 1. Position of the Ghost cells (interpolation points) in Immersed Boundary Method for a cylinder.

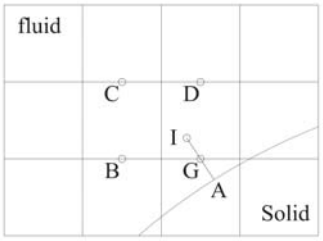

Figure 2. Algorithm to decide the value of the Ghost cell with surrounding points by Immersed Boundary Method.

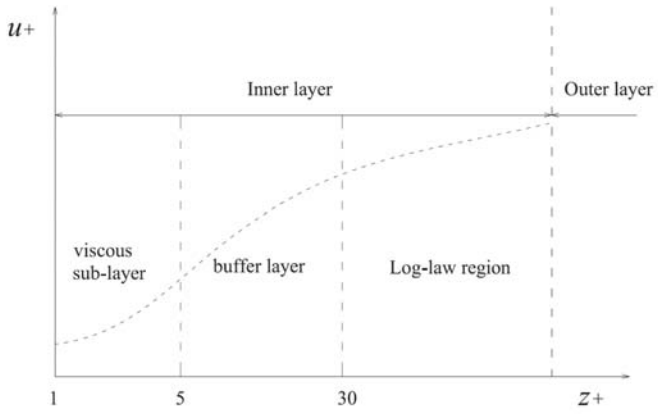

Figure 3. Wall modeling. Relationship between z_+ and u_+ is decided by each flow regime.

Turbulence model

To predict instantaneous flow characteristics around a cylinder, which is important to obtain appropriate bulk drag coefficient, a turbulence model Large Eddy Simulation is incorporated into CADMAS-SURF/3D. Smagorinsky model (Christensen and Deigaard 2001, Suzuki and Okayasu 2004) is selected as the SGS (Sub grid scale) model in this study. The eddy viscosity is shown as follows.

$$\nu_t = l_{mix}^2 \sqrt{2\overline{S}_{ij}\overline{S}_{ij}} \tag{4}$$

$$\overline{S}_{ij} = \frac{1}{2}\left(\frac{\partial u_i}{\partial x_j} + \frac{\partial u_j}{\partial x_i} \right) \tag{5}$$

$$l_{mix} = C_s \Delta = C_s \sqrt[3]{\Delta x \Delta y \Delta z} \tag{6}$$

where C_s is the Smagorinsky constant and set as 0.10 in this study.

Basic equations

A VOF model CADMAS-SURF/3D based on the three dimensional Navier-Stokes equation has been applied to this study. This model can deal with the effects of free surface and wave breaking, and provide information of water surface elevation, wave velocity, wave acceleration and wave pressure for each cell. This model is programmed to be able to conduct a parallel computation.

The basic equations including the Immersed Boundary Method and Large Eddy Simulation are as follows.

The continuity equation:

$$\frac{\partial \gamma_x u}{\partial x} + \frac{\partial \gamma_y v}{\partial y} + \frac{\partial \gamma_z w}{\partial z} = \gamma_v S_p \tag{7}$$

The momentum equation:

$$\begin{aligned}
&\lambda_v \frac{\partial u}{\partial t} + \frac{\partial \lambda_x uu}{\partial x} + \frac{\partial \lambda_y vu}{\partial y} + \frac{\partial \lambda_z wu}{\partial z} = -\frac{\gamma_v}{\rho}\frac{\partial p}{\partial x} \\
&+ \frac{\partial}{\partial x}\left\{ \gamma_x \nu_e \left(2\frac{\partial u}{\partial x} \right) \right\} + \frac{\partial}{\partial y}\left\{ \gamma_y \nu_e \left(\frac{\partial u}{\partial y} + \frac{\partial v}{\partial x} \right) \right\} + \frac{\partial}{\partial z}\left\{ \gamma_z \nu_e \left(\frac{\partial u}{\partial z} + \frac{\partial w}{\partial x} \right) \right\} + S_u - R_x + f_x \\
&\lambda_v \frac{\partial v}{\partial t} + \frac{\partial \lambda_x uv}{\partial x} + \frac{\partial \lambda_y vv}{\partial y} + \frac{\partial \lambda_z wv}{\partial z} = -\frac{\gamma_v}{\rho}\frac{\partial p}{\partial x} \\
&+ \frac{\partial}{\partial x}\left\{ \gamma_x \nu_e \left(\frac{\partial v}{\partial x} + \frac{\partial u}{\partial y} \right) \right\} + \frac{\partial}{\partial y}\left\{ \gamma_y \nu_e \left(2\frac{\partial v}{\partial y} \right) \right\} + \frac{\partial}{\partial z}\left\{ \gamma_z \nu_e \left(\frac{\partial v}{\partial z} + \frac{\partial w}{\partial y} \right) \right\} + S_v - R_y + f_y \\
&\lambda_v \frac{\partial w}{\partial t} + \frac{\partial \lambda_x uw}{\partial x} + \frac{\partial \lambda_y vw}{\partial y} + \frac{\partial \lambda_z ww}{\partial z} = -\frac{\gamma_v}{\rho}\frac{\partial p}{\partial z} \\
&+ \frac{\partial}{\partial x}\left\{ \gamma_x \nu_e \left(\frac{\partial w}{\partial x} + \frac{\partial u}{\partial z} \right) \right\} + \frac{\partial}{\partial y}\left\{ \gamma_y \nu_e \left(\frac{\partial w}{\partial y} + \frac{\partial v}{\partial z} \right) \right\} + \frac{\partial}{\partial z}\left\{ \gamma_z \nu_e \left(2\frac{\partial w}{\partial z} \right) \right\} + S_w - R_z - \gamma_v g
\end{aligned} \tag{8}$$

where t is time, x, y, z are the coordinates, u, v, w are the large scale velocity vector, ρ is the water density, p pressure, ν_e the kinematic viscosity (summation of the molecular viscosity ν and eddy viscosity ν_t), g is the gravitational acceleration, γ_v is the porosity, and γ_x, γ_z, γ_z are the permeability. f_x, f_y are external force in Immersed Boundary Method. S_p, S_u, S_v, S_w are source terms for wave generation. λ_v, λ_x, λ_y, λ_z are expressed by using the inertia coefficient C_M as below:

$$\begin{aligned}
\lambda_v &= \gamma_v + (1-\gamma_v)C_M \\
\lambda_x &= \gamma_x + (1-\gamma_x)C_M \\
\lambda_y &= \gamma_y + (1-\gamma_y)C_M \\
\lambda_z &= \gamma_z + (1-\gamma_z)C_M
\end{aligned} \tag{9}$$

R_x, R_y and R_z are resistance terms for a porous structure:

$$R_x = \frac{1}{2}\frac{C_D}{\Delta x}(1-\gamma_x)u\sqrt{u^2+v^2+w^2}$$
$$R_y = \frac{1}{2}\frac{C_D}{\Delta y}(1-\gamma_y)v\sqrt{u^2+v^2+w^2} \quad (10)$$
$$R_z = \frac{1}{2}\frac{C_D}{\Delta z}(1-\gamma_z)w\sqrt{u^2+v^2+w^2}$$

where Δx, Δy, Δz are the size of the calculation grid, and C_D is the drag coefficient. In this study, the effect of λ and R are not included since there is no porous media in this study.

As a time integration method, the second-order explicit Adams-Bashforth scheme is incorporated into CADMAS-SURF/3D so as to keep second-order accuracy for time domain as used in spatial domain. In this case, to maintain the accuracy, each time step dt is fixed in the calculations. The equation is as below.

$$u^{n+1} = u^n + \Delta t\left\{1.5\left(-ADV + DIFF\right)^n - 0.5\left(-ADV + DIFF\right)^{n-1} - \nabla p^{n+1}\right\} \quad (11)$$

where n is step, ADV and $DIFF$ are advection terms and diffusion terms respectively.

VALIDATION OF THE MODEL

A lot of physical experiments and numerical simulations about flow around a circular cylinder have been carried out that seem suitable for validation of this model. In this section, the numerical experiments are compared with results from literature.

Flow with *Re*=300

To validate the current model, a case of three dimensional flow around a circular cylinder with *Re*=300 is selected since several numerical experiment results are available in literature (Mittal and Barachander 1997, Kravchenko et al. 1999). These numerical simulations use body fitted grids. Specifically drag coefficient, root-mean-square lift coefficient and Strouhal number are investigated in this validation. The entire boundary flow regime in the Ghost cell in this case is sub-viscous layer, so the relationship between u_+ and z_+ is as shown in Equation (1).

A numerical open channel is developed to conduct numerical experiments. The length, width and height are 0.96 m (32 D; D=0.03 m is a diameter of a cylinder located in the numerical open channel), 0.51 m (17 D), 0.18 m (6 D), respectively. In this case *Re*=300, vortex shedding in the turbulent wake regime (i.e. Re>200) occurs along the length of the cylinder (Sumer and Fredsøe 2006). According to Gerlach and Dodge (1970), the correlation length is 2-3 D in the flow with $150<Re<10^5$. Therefore the numerical channel is set as three-dimensional and takes 6 D in the vertical axis as being enough to accommodate the three-dimensional effect. The grid size near the cylinder is 0.001 m, and the total number of grid points is $336 \times 192 \times 60$=3,870,720. The grid size is fine around the cylinder and coarser for the region away from the cylinder. In this case, VOF model is not used because there is no water surface in this calculation. The velocity of the inflow from the boundary is 0.01 m/s with perturbation. A slip boundary condition is applied to the side wall and a convective boundary condition is used at the outflow boundary as shown in Equation (12). Statistics are computed by averaging in time over 12 shedding cycles.

$$\frac{\partial u_i}{\partial t} + u_\infty \frac{\partial u_i}{\partial x} = 0 \quad (12)$$

Table 1 shows the result of this numerical simulation, which are averaged drag coefficient, root-mean-square lift coefficient and Strouhal number. As shown in the Table 1, it is confirmed that the result in the present study is almost the same as the results from literature (Mittal and Barachander 1997, Kravchenko et al. 1999, Balaras 2004). The variation of the lift and drag coefficients with time is shown in Figure 4. These have same tendency with the result shown in Balaras (2004). Mean velocity

profiles and time averaged velocity fluctuations at three downstream locations from the cylinder center shown in Figure 5 also correspond to the results of spectral simulations in Mittal and Balachandar (1997).

From these results, it can be concluded that the present model has the ability to represent the flow conditions when the Reynolds number is 300.

Table 1. Flow parameters (drag coefficient, lift coefficient and Strouhal number) of the circular cylinder in the case of *Re*=300.

CASE	C_D	C_{Lrms}	*St*
Mittal and Balachander (Spectral method)	1.26	0.38	0.203
Kravchenko et al. (Bi-spline method)	1.28	0.40	0.202
Balaras (Immersed Boundary Method)	1.27	0.42	0.21
Present study	1.30	0.40	0.21

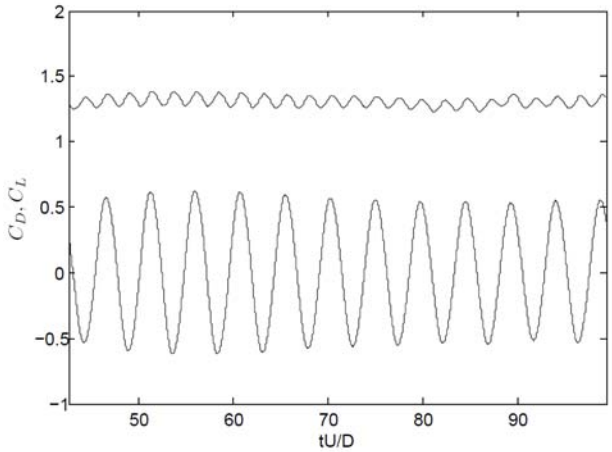

Figure 4. Variation of the drag and lift coefficients with time in the case of *Re*=300.

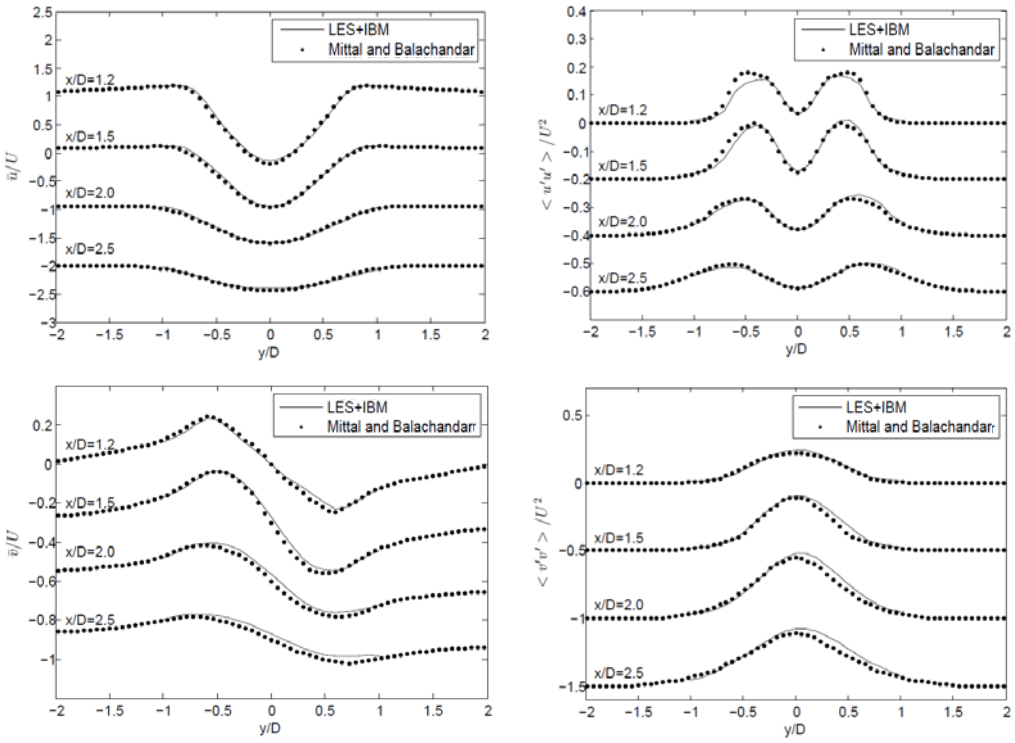

Figure 5. Mean velocity profiles and time averaged velocity fluctuations at four downstream locations form the cylinder center spectral simulation Mittal and Balachandar in the case of *Re*=300.

Flow with *Re*=3,900 and 8,000

The case with *Re*=300 is successful though the Reynolds number is still relatively low. To make sure the result is valid for relatively high Reynolds number, two other cases are additionally conducted. One is for *Re*=3,900 and the other one for *Re*=8,000. The inflow velocities are changed to adjust the Reynolds number, and the other conditions remain the same. In these cases, the number of grid points across the boundary layer becomes less compared to the case with *Re*=300 as the flow becomes faster. Therefore the boundary flow regime in the Ghost cell in this case is not always sub-viscous layer, but also buffer layer and Log-law region. Each boundary condition is decided by the flow velocity and distance between the calculation point and the cylinder surface.

Table 2 shows the result of drag coefficient and Strouhal number in *Re*=3,900. As shown in Table 2, it is also confirmed that the present result is in good agreement with the results in literature (Norberg 1994, Blackburn and Schmidt 2001) in terms of averaged drag coefficient and Strouhal number. The differences are within 5 %. Figure 6 shows distribution of average velocity in the center line behind the cylinder (left) and Reynolds normal stress in cross-sectional line at 6 different points behind the cylinder (right). As for the average velocity, numerical results obtained in this study and Laurenco and Shih (1993) are in good agreement with data from 0.5 *x/D* to 2.0 *x/D*. The tendency is slightly different in the range 2.0 *x/D* to 3.5 *x/D*, however, the numerical result matches with that of Ong and Wallace (1996). In the range 3.5 *x/D* to 4.2 *x/D*, the numerical results are fitted to both Laurenco and Shih (1993) and Ong and Wallace (1996). Since there are some gaps even between these flume experimental results, it can be said that the result obtained here is in good agreement with experimental data. As for the result of Reynolds normal stress, a slight difference can be seen between numerical results and experimental results but in general their tendency is the same. Table 3 shows the results for drag coefficient and Strouhal number in *Re*=8,000. In this case, the resolution to a boundary layer is more rough compared to *Re*=3,900 as the inflow velocity is faster. However, this result is still also reasonably fitted to the reference data in Sumer and Fredsøe (2006). Note that there is no measurement data which can be compared to this study for velocity field as far as we know.

From the results shown above, it can be concluded that the model in this study, the present model can reproduce the flow around a cylindrical structure and drag coefficient in a Cartesian grid properly even though the Reynolds numbers of these cases (*Re*=3900 and 8,000) are rather higher than the ones in Balaras (2004).

Table 2. Flow parameters (drag coefficient and Strouhal number) of the circular cylinder in the case of *Re*=3,900.

CASE	C_D	*St*
Norberg (Experiment)	0.99	0.210
Blackburn and Schmidt (Spectral method)	1.01	0.218
Present study	0.98	0.22

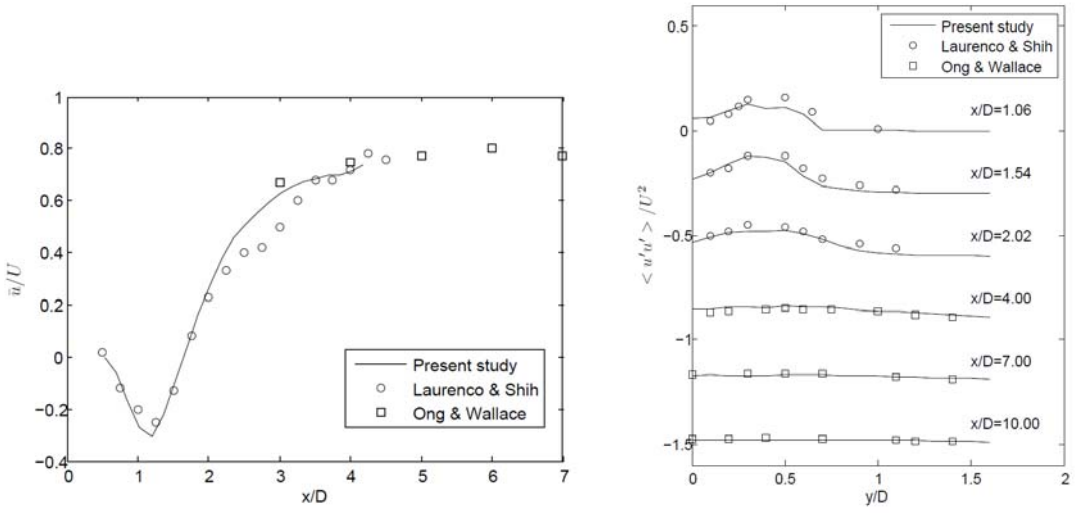

Figure 6. Distribution of average velocity in the center line behind the cylinder (left) and Reynolds normal stress in cross-sectional line at 6 different points behind the cylinder (right)

Table 3. Flow parameters (drag coefficient and Strouhal number) of the circular cylinder in the case of *Re*=8,000.

CASE	C_D	*St*
Experiment results extracted from Sumer and Fredsøe (2006)	1.1	0.212
Present study	1.05	0.22

BULK DRAG COEFFICIENT

Numerical experiment

In the last section, it was shown that the present model can reproduce the flow around a cylinder and the force acting on the cylinder. Therefore, it is assumed that the present model is capable of reproducing the flow in multiple cylinders under wave condition. In this section, bulk drag coefficient over multiple cylinders under wave condition is investigated.

A numerical wave channel is developed to conduct the numerical experiments. The length, width and height are 16.0 m, 0.5 m and 0.15 m, respectively. The diameter of each cylinder is 0.05 m and height is 0.08 m. The cylinders are allotted in three different densities in the numerical wave channel as shown in Figure 7. The densities are *S/D*=2.8, 2.0 and 1.4 respectively (*S* represents the distance between cylinders and D is diameter of a cylinder). and *n*=1.0 for the three cases (*n* in the figure represents ratio of longitudinal to lateral low spacing). The total number of grids is $800\times100\times15$=1,600,000. The water depth is set as 0.10 m, the incident wave height is 0.02 m and wave period is 2.0 s at the wave boundary. The wave height is set relatively small to avoid the influence of breaking and also to be able to apply the small amplitude theory for analysis. A 4 m width sponge layer is introduced at the end of the wave channel to decrease the effect of the reflection from the end of the boundary. In this case, VOF model is used for the water surface and to evaluate wave energy dissipation through multiple cylinders by wave height attenuation.

Measurements of the water surface elevations are conducted along the longitudinal center line of the wave flume for 68 points. For each run, 3 consecutive waves are selected for analysis after a time at which a stable incident wave arrived at each wave gauge. The wave heights in front of and behind the multiple cylinders are calculated by the spatial averages. Specifically, the incident wave heights are calculated by the average of the wave heights in front of the multiple cylinders and the attenuated wave heights behind the multiple cylinders are calculated by the average of the wave heights in one wave length where the wave height distribution becomes stable. Finally bulk drag coefficient is calculated based on wave height differences and distance of the multiple cylinders.

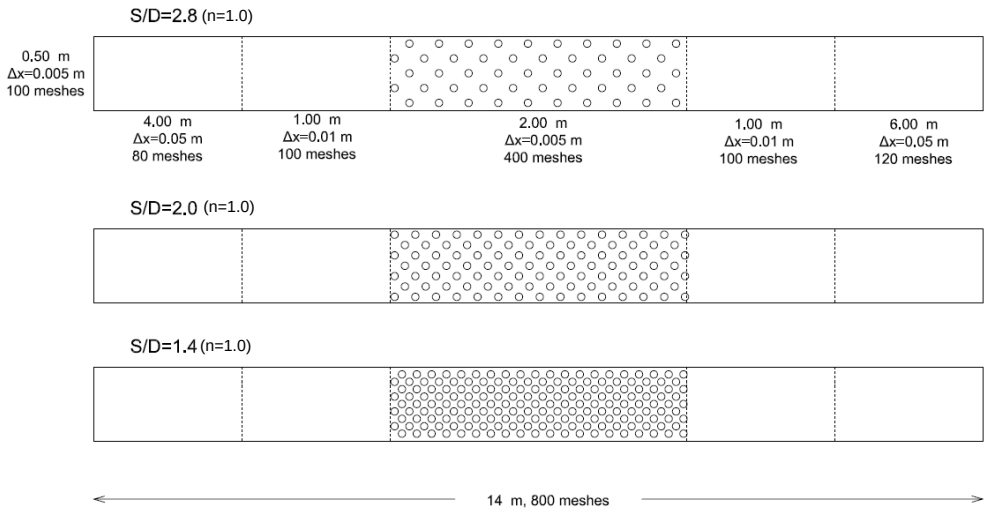

Figure 7. Three different configurations of cylinder density. The densities of cylinder array is S/D=2.8 (N=50), S/D=2.0 (N=100) and S/D=1.4 (N=200), respectively.

Table 4 shows results for bulk drag coefficients in different densities along with a single drag coefficient when *KC*=5, *Re*=6,250 and beta=1,250. The single drag coefficient is obtained by a numerical simulation with a cylinder placed in the center of the numerical wave channel. The drag coefficient is calculated by a least square method like in Sumer and Fredsøe (2006), and the result corresponds to the value obtained by Sarpkaya (1976) in his physical experiment. As for the bulk drag coefficient in the multiple cylinders, the value for *S/D*=2.8 and *S/D*=2.0 were almost the same as the drag coefficient of a single cylinder. However when the density reaches to *S/D*=1.4, the bulk drag coefficient decreases by 13 %.

Table 4. Drag coefficient for a single cylinder and bulk drag coefficients in the different densities for multiple cylinders.

CASE	C_D or Bulk drag coefficient
Single cylinder	1.4
S/D=2.8 (N=50)	1.39
S/D=2.0 (N=100)	1.40
S/D=1.4 (N=200)	1.22

Discussion

According to Massel et al. (1999), decrease of the drag coefficient by multiple cylinders is a function of density and Reynolds number. However, the bulk drag coefficients obtained in this study do not change so much even when the spatial densities of these cases are quite high. Only the bulk drag coefficient with the case of *S/D*=1.4 decreases slightly.

Since the number of obtained numerical simulation results is limited for 3 cases and the data consist of only one *KC* number (*KC*=5), flume experiment data obtained by the first author are added to this analysis. Figure 9 shows the bulk drag coefficients from the numerical simulation in the present study (low *KC* number), bulk drag coefficients from the flume experiment (high *KC* number) and the bulk drag coefficient lines from Nepf (1999). The vertical axis represents the bulk drag coefficient of multiple cylinders divided by drag coefficient of single cylinder in order to evaluate the effect of the interference of cylinders. The horizontal axis is a dimensionless population density (*ad* is equal to D^2/S^2). The numerical simulation results and the flume experiment results are obtained under wave conditions and Nepf (1999)'s results are obtained under flow conditions. The results of Nepf (1999) indicate that bulk drag coefficient is a function of density (*ad*) and cylinder array (*n*) for a steady flow case. From the result of the numerical simulation and the flume experiment, it can be said that bulk drag coefficient in multiple cylinder is related not only to density but also *KC* in case of wave conditions. It seems that the bulk drag coefficients become small when *KC* becomes large.

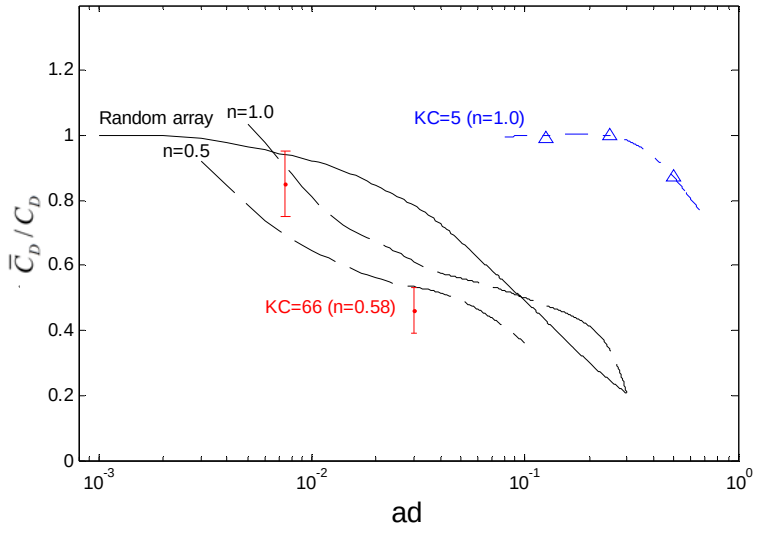

Figure 8. Ratio of bulk drag coefficient to drag coefficient versus dimensionless population density. The black lines represent Nepf (1999) under flow conditions, the blue plots are the present numerical results and the red plots are the flume experiment results under wave conditions.

To obtain more insights into the nature of the bulk drag coefficient, a parameter 2*a* is introduced here. 2*a* represents stroke of the motion which is shown in Equation (13) by using the small amplitude theory. Since *KC* is described as Equation (14) also by using the small amplitude theory, 2*a* is expressed as Equation (15). From the equation, it is found that 2*a* is linearized by *KC* when *D* is fixed.

$$2a = H\frac{\cosh k(h+y)}{\sinh kh} \tag{13}$$

$$KC = \frac{\pi H}{D}\frac{\cosh k(h+y)}{\sinh kh} \tag{14}$$

$$2a = \frac{KC}{\pi}D \tag{15}$$

Figure 9 is a redraw of wave condition data in Figure 8, which uses non-dimensional parameter 2*a/S* in x-axis. As can be seen in Figure 9, the numerical results and the flume experimental results are on a same trend, in which the ratio of bulk drag coefficient to drag coefficient become small when 2*a/S* increases. The trend seems to start from 2*a/S*=1. Therefore, even when the density is very big, the ratio of bulk drag coefficient to drag coefficient does not change if the stroke of the motion is even smaller. On the contrary, even the density is very small, the ratio of bulk drag coefficient to drag coefficient changes when the stroke of the motion is larger than the distance.

These results lead to the fact that the ratio of bulk drag coefficient to drag coefficient is not a function of *S/D*, but would be a function of 2*a/S*. However, it has to be noted that this non-dimensional parameter 2*a/S* does not include the effect of the diameter of cylinder, which might affect the bulk drag coefficient, so it is necessary to conduct a further investigation.

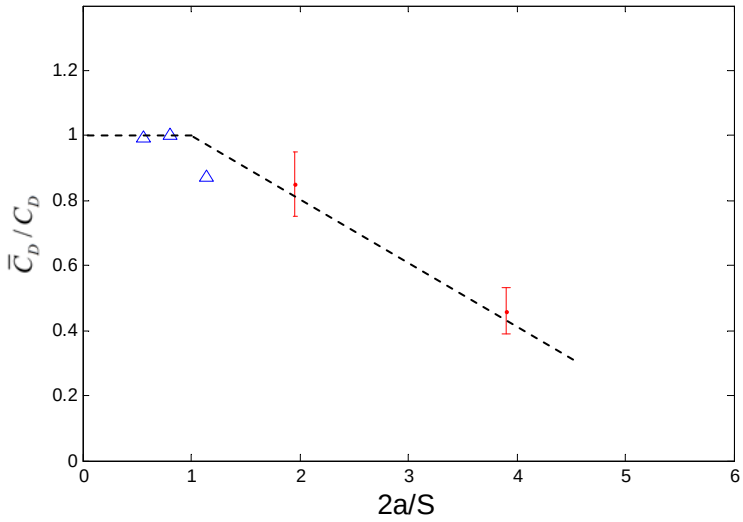

Figure 9. Ratio of bulk drag coefficient to drag coefficient versus non-dimensional parameter 2*a/S*.

CONCLUSIONS

Bulk drag coefficient in rigid dense vegetation was investigated mainly by using a three dimensional numerical simulation model CADMAS-SURF/3D by incorporating Immersed Boundary Method and Large Eddy Simulation. From the validation, all the results obtained in this paper (*Re*=300, 3,900 and 8,000) show good agreement with the reference data in literature, which indicates that the models developed for this study were successfully installed and can reproduce the flow around a cylinder and drag coefficient in Cartesian grid.

From the numerical simulation of bulk drag coefficient in multiple cylinders, it was concluded that the ratio of bulk drag coefficient of multiple circular cylinders to drag coefficient of a single

circular cylinder, which represents a reduction, is not just a function of density but a function of parameter $2a/S$, in which $2a$ is stroke of the motion and S is cylinder distance. When $2a$ is less than S, the effect of the density is neglected because the wake does not reach the other cylinders even when the density is high. On the contrary, it might affect the ratio of bulk drag coefficient to drag coefficient when the stroke of the motion is larger than the cylinder distance even if the density is low. In general, the ratio of bulk drag coefficient to drag coefficient becomes low when $2a/S$ becomes high. However, it is assumed that the reduction in drag coefficient, namely the ratio of bulk drag coefficient to drag coefficient, has a lower limit because the bulk drag coefficient in oscillation flow for the very large $2a/S$ would become similar to the one in flow like in Nepf (1999). In this study it was not possible to define the rate of drag coefficient decrease because of data limitations and the variety of KC and Re was limited. However, it is necessary for further study in this subject to improve the estimation of wave dissipation over multiple cylinders such as in mangrove forests (Narayan 2009) and shrub communities (de Oude et al. 2010).

RECCOMENDATIONS

- In this study, the number of the calculation is limited to 3 cases and these cases are also limited to small KC number (KC=5). It is necessary to investigate more cases with variable KC numbers so as to cover wide range of $2a/S$.
- According to Nepf (1999), bulk drag coefficient depends on the array of cylinders. Therefore the effect of the configuration of the array also needs to be investigated.
- It has to be noted that this non-dimensional parameter $2a/S$ does not include the effect of the diameter of cylinders, which might affect the bulk drag coefficient, so it is necessary to conduct a further investigation.
- Since this model can be extended to movable structures, it might be possible to conduct a simulation for flexible vegetation.

ACKNOWLEDGMENTS

The first author (T. Suzuki) was supported by a scholarship awarded by the Rotary Foundation and Het Lammingafonds and currently is supported by Water Research Center Delft. These financial supports are gratefully acknowledged.

REFERENCES

Arikawa, T., F. Yamada, M. Akiyama, 2005. Study of the Applicability of Tsunami Wave Force in a Three-Dimensional Numerical Wave Flume. *Annual Journal of Coastal Engineering*, JSCE, Vol.52: 46-50. (in Japanese)

Arikawa, T., T. Yamano and M. Akiyama, 2007. Advanced Deformation Method for Breaking Waves by using CADMAS-SURF/3D, *Annual Journal of Coastal Engineering*, JSCE, Vol54: 71-75. (in Japanese)

Augustin, L., Jennifer L. Irish, Patrick Lynett, 2009. Laboratory and numerical studies of wave damping by emergent and near-emergent wetland vegetation, *Coastal Engineering* 56 (2009) 332–340.

Balaras, Elias, 2004. Modeling complex boundaries using an external force field on fixed Cartesian grids in large-eddy simulations, *Computers & Fluids* 33 (2004) 375–404.

Blackburn, H. M. and Schmidt, S., 2001. Large eddy simulation of flow past a circular cylinder. *In 14th Australasian Fluid Mechanics Conference.*

Briscolini, M. and Santangelo, P., 1989. Development of the mask method for incompressible unsteady flows. *Journal of Computational Physics*, 84(1):57 – 75.

Christensen, E.D., Deigaard, R., 2001. Large eddy simulation of breaking waves. *Coastal Engineering* 42: 53–86.

de Oude, R., D.C.M. Augustijn, F. D., Wijnberg, K., de Vries, M., and Suzuki, T., 2010. Modelling wave attenuation by vegetation in swan to determine a vegetation field for decreasing dike height in the noordwaard, the netherlands. *ISEH 2010*.

Fadlun, E. A., Verzicco, R., Orlandi, P., and Mohd-Yusof, J., 2000. Combined immersed-boundary finite-difference methods for three-dimensional complex flow simulations. *Journal of Computational Physics*, 161(1):35 – 60.

Goldstein, D., Handler, R., and Sirovich, L., 1993. Modeling a no-slip flow boundary with an external force field. *Journal of Computational Physics*, 105(2):354 – 366.

Heideman, J. and Sparpkaya, T., 1985. Hydrodynamic forces on dense arrays of cylinders. *OTC1985*.

Iimura, K., Tanimoto, K., Hien, N. X., Akagawa, Y., and Yutani, K., 2007. Numerical simulation of ship wave damping by emergent vegetation community. *Annual Journal of Coastal Engineering*, JSCE, 54:766–770. (in Japanese)

Kobayashi N., Raichle A.W. & Asano, T., 1993. Wave attenuation by vegetation. *J. Waterw. Port Coast. Ocean Eng*. 119, 30-48.

Kravchenko, A. G., Moin, P., and Shariff, K., 1999. B-spline method and zonal grids for simulations of complex turbulent flows. *J. Comput. Phys.*, 151(2):757– 789.

Lourenco, L. M. and Shih, C., 1993. Characteristics of the plane turbulent near wake of a circular cylinder; a particle image velocimetry study (data taken from Beaudan & Moin 1994).

Mendez F.M. & Losada I.J., 2004. An empirical model to estimate the propagation of random breaking and nonbreaking waves over vegetation fields. *Coastal Engineering* 51, 103-118.

Mittal, R. and Balachandar, S., 1997. On the inclusion of three-dimensional effects in simulations of two-dimensional bluff body wake flows. *In Proceedings of ASME Fluid Engineering Division Summer Meeting*, Vancouver, BC, Canada.

Mohd-Yusof J. 1997. Combined immersed boundaries/B-splines methods for simulations of flows in complex geometries. *CTR Annual Research Briefs, NASA* Ames/Stanford University.

Narayan, S., 2009. The effectiveness of mangroves in attenuating cyclone- induced waves. Master's thesis, *Delft University of Technology*.

Nepf., H. M., 1999. Drag, turbulence, and diffusion in flow through emergent vegetation, *Water resources research*, vol. 35, No. 2: 479-489.

Norberg, C., 1994. An experimental investigation of the flow around a circular cylinder: influence of aspect ratio. *Journal of Fluid Mechanics Digital Archive*, 258(-1):287–316.

Ong, L. and Wallace, J., 1996. The velocity field of the turbulent very near wake of a circular cylinder. *Experiments in Fluids*, 20:441–453.

Peskin. C. S., 1972. Flow patterns around heart valves: A numerical method, *Journal of Compt. Phys*., 10-2, pp.252-271

Sarpkaya, T., 1976. Vortex shedding and resistance in harmonic flow about smooth and rough circular cylinders at high Reynolds numbers. *Tech. Rep. No. NPS-59SL76021*, Naval Postgraduate School, Monterey, CA.

SPM (Shore Protection Manual). 1984. Coastal Eng. Res. Center, U.S. Army Corps of Engineers, Washington, vol. I.

Sumer, B.M., J. Fredsøe, 2006. *Hydrodynamics around cylindrical structures. Revised Edition*, World Scientific.

Suzuki, T., T. Arikawa and Marcel J.F. Stive, 2009. Numerical modeling of hydrodynamics in a salt marsh. *Proceedings of Coastal dynamics 2009*, ASCE.

Suzuki, T., Okayasu, A., and Shibayama, T., 2007. A numerical study of intermittent sediment concentration under breaking waves in the surf zone. *Coastal Engineering*, 54(5):433 – 444.

Yang, J. and Balaras, E., 2006. An embedded-boundary formulation for large eddy simulation of turbulent flows interacting with moving boundaries. *Journal of Computational Physics*, 215(1):12 – 40.